Taylor & Francis
Taylor & Francis Group

Mechanics Based Design of Structures and Machines

An International Journal

ISSN: 1539-7734 (Print) 1539-7742 (Online) Journal homepage: https://www.tandfonline.com/loi/lmbd20

Integrated structure/control design of high-speed flexible robot arms using topology optimization

Mohamed G. Alkalla & Mohamed A. Fanni

To cite this article: Mohamed G. Alkalla & Mohamed A. Fanni (2019): Integrated structure/control design of high-speed flexible robot arms using topology optimization, Mechanics Based Design of Structures and Machines, DOI: 10.1080/15397734.2019.1688170

To link to this article: https://doi.org/10.1080/15397734.2019.1688170

MECHANICS BASED DESIGN OF STRUCTURES AND MACHINES
https://doi.org/10.1080/15397734.2019.1688170

Integrated structure/control design of high-speed flexible robot arms using topology optimization

Mohamed G. Alkalla[a,b] and Mohamed A. Fanni[b,c]

[a]Surrey Space Centre, University of Surrey, Guildford, UK; [b]Production Engineering & Mechanical Design Department, Mansoura University, Mansoura, Egypt; [c]Mechatronics and Robotics Engineering Department, Egypt-Japan University of Science and Technology (E-JUST), Alexandria, Egypt

ABSTRACT

Most robotic applications demand lightweight and high-speed manipulators for considerably reducing the consumed power and achieving high production rates. The two ways for seeking such high-speed arms are; applying advanced control algorithms and/or performing an extensive optimization of the arm structure itself. Therefore, the topology optimization technique is proposed here for obtaining an optimal robot arm design from both structure and control viewpoints. Results of some researches, that have been previously accomplished by size and shape optimization, were encouraging enough to extend and propose this optimization approach. The method of moving asymptotes (MMA) as an optimization algorithm, the finite element analysis (FEA) by ANSYS, and the time-optimal control method are integrated to gain an optimum design capable of attaining the minimum traveling time. The proposed methodology focuses on performing different comparisons between the proposed optimum topological designs and their initial designs for different robot arms' sizes and materials. It also distinguishes between the proposed optimum design and the previously achieved one by size optimization under the same operational conditions. Therefore, the significance of the proposed technique is emphasized. It shows that the traveling time is reduced by 44.8%, while the previous work only achieved 23.5%. In addition, the mass is reduced to nearly half of its initial value, taking into account the air damping as the real case in all terrestrial applications.

ARTICLE HISTORY
Received 3 January 2019
Accepted 30 October 2019

KEYWORDS
Flexible robot arm; topology optimization; method of moving asymptotes; bang-bang; time optimal control

1. Introduction

Nowadays, lightweight and high-performance robotic arms are very demanded in many fields including; industrial, aerospace, and orbital/space manipulators, where, some substantial requirements should have existed, such as; high operational speed, accuracy, and payload/weight ratio, Gao and Wang (2003). Additionally, the need for lightweight manipulators to be mounted on the autonomous mobile robots, where power limitations are imposed by the battery, has to be taken into consideration. Unfortunately, the flexibility of these lightweight arms leads to oscillatory behavior at their tips. This makes the precise pointing or tip positioning a difficult task which requires a complex closed-loop control. Most current approaches aim at decreasing the end-effector residual vibration by improving the structural design of the robot arm or adopting

CONTACT Mohamed G. Alkalla m.alkalla@surrey.ac.uk; m_elkalla@mans.edu.eg Surrey Space Centre, University of Surrey, Guildford, GU2 7XH, UK.
Color versions of one or more of the figures in the article can be found online at www.tandfonline.com/lmbd.
Supplemental data for this article can be accessed on the publisher's website.
Communicated by John McPhee.

advanced control techniques. Feedforward and feedback control strategies, studied by Wells et al. (1990) showed that, by compensating for the dynamics of both the servo and the arm, a good response of the flexible arm was obtained since the feedforward only has limitations on getting the final target position. They illustrated that positional and accelerometric feedback combined with PD compensator acting on the position error, is a viable solution in the less stable situation rather than using feedback control only. (De Luca et al. 1990; De Luca and De Simone 1997; De Luca 2000) proposed the same strategy but with using a state observer along with a high-order polynomial trajectory instead of using sensors. They reported that the output trajectory has a bang-bang acceleration profile for a two-link manipulator slew motion. On the other hand, Asada et al. (1990) proposed a method based on virtually rigid link coordinate systems to solve the inverse dynamics problem of a flexible planar arm. Furthermore, Carrera and Serna (1996) proposed an inverse-dynamics based method to find the joint actuating torques which must be applied to obtain a specified end-effector trajectory. This has been accomplished by coupling the elastic deformations of the arms and the rotations at the joints into the inverse dynamics model. Lai and Dopker (1990) proposed a computational method for the dynamics analysis of flexible multi-body mechanisms taking into account the influence of lumped rotary inertia. Hong and sik Park (1999) presented a vibration-reducing technique concerning the motion-induced vibration of a flexible manipulator. Their proposed torque wheel reduces the vibration and cancels the motion-induced force. It is based on the dynamic modeling of the manipulator rather than the structural design of the links themselves. Bhattacharya et al. (2018) proposed a one-dimensional flexible structure consists of rigid segments with 1-DOF rotary joints like the spine of the animal whose substantial deformation allows the body to move efficiently and achieve high speeds. They found that changing the orientation or the shape of the one-dimensional structure has more effect than changing the joints' stiffness. Therefore, the structural design is very crucial aspect for achieving the high-speed motion. Whilst, most recent researches focus on developing the controller design of flexible robot arms, such as; Zhang et al. (2018), Zhang (2018), Yamaguchi et al. (2018), Kayastha et al. (2018), and Dong et al. (2019), a few of them concentrates on optimizing the arm structure itself, such as:

- Optimizing the weight to stiffness ratio by varying the length and cross-section of each link using size optimization, as presented by Imam and Sandor (1975). Also, applying size optimization by variable hole sizes embedded into the link integrated with controller design, as presented by Fanni and El-Keran (2000).
- Utilizing advanced composite material for the arm structural design, as presented by Ghazavi and Gordaninejad (1995).
- Applying shape optimization on flexible robotic manipulator, as studied by Asada et al. (1991) and Dixit et al. (2006).

Contrary to the previous works, the topology optimization technique is proposed here for obtaining an optimum structural arm design integrated with time-optimal control theory. This approach leads to optimum robotic arm design from both structure and control prospectives, since the proposed approach concerns with improving both the controller and structural design simultaneously. This paper is organized as follows: Section 2 describes the time-optimal control theory (Bang-Bang control) for air damped and undamped models. Section 3 explains the structural topology optimization concept and the method of moving asymptotes as the main optimization algorithm. Section 4 presents a formulation of the constrained optimization problem resulted from the fusion of topology optimization technique and time-optimal control theory. Finally, the results of topology optimization for different flexible robot arms including comparisons with the previously-used size optimization are illustrated in Section 5.

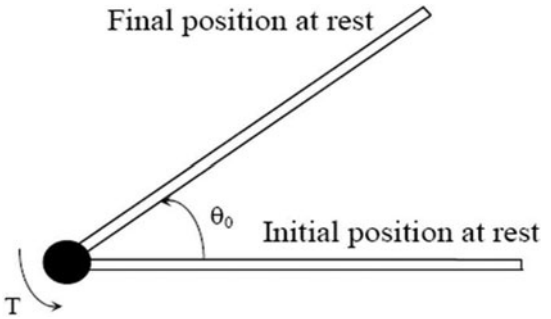

Figure 1. Flexible robot arm layout.

2. Time-optimal control of flexible robot arm

2.1. Mathematical model without air damping

The application of time-optimal control theory for obtaining a minimum traveling time of the flexible robot arm results in a multi-switch bang-bang control. The problem can be formulated as follows: Given a single flexible link rotates in a horizontal plane and an actuator with a maximum torque T_o. Therefore, how should the actuating torque vary with time to make the arm rotates in minimum time by a given angle θ_o from initial to final rest state, as shown in Figure 1. The arm model is represented by one rigid and one flexible mode with the following state equation without considering the air damping as:

$$\dot{\mathbf{x}}(t) = \mathbf{A}\mathbf{x}(t) + \mathbf{b}T(t) \tag{1}$$

$$\mathbf{A} = \begin{bmatrix} 0 & 1 & 0 & 0 \\ 0 & 0 & 0 & 0 \\ 0 & 0 & 0 & 1 \\ 0 & 0 & -\omega^2 & 0 \end{bmatrix}, \mathbf{b} = \begin{bmatrix} 0 \\ b_o \\ 0 \\ b_1 \end{bmatrix} \tag{2}$$

where $\mathbf{x}(t)$ is the modal coordinate vector, $T(t)$ is the actuating torque, ω is the natural frequency of the flexible mode, b_o is the component of weighted rigid mode shape at a coordinate where the torque is applied, and $(1/b_o)^2 = J$, where, J is the mass moment of inertia of the arm about its rotating axis, b_1 is similar to b_o but for flexible mode shape, and ${b_1}^2 = q$, where, q is the flexible mode participation factor, as stated by Park and Asada (1994). Both b_o and b_1 can be obtained using finite element method (FEM). Through applying the Pontryagin maximum principle, the optimal solution is found to be a multi-switch bang-bang control, as presented by (Pao and Franklin 1990; Fanni 2000) and shown in Figure 2. It shows that the three switches $(t_f/2 - t_a), (t_f/2)$ and $(t_f/2 + t_a)$ are symmetrical about the middle switch, so, it is only required to calculate t_a and t_f from the following two equations:

$$\left(\frac{t_f}{2}\right)^2 - 2t_a^2 = \frac{\theta_o J}{T_o} \tag{3}$$

$$\cos\left(\frac{\omega t_f}{2}\right) - 2\cos(\omega t_a) + 1 = 0 \tag{4}$$

where t_f is the optimal traveling time from initial to final rest and it depends on both the mass moment of inertia J and the natural frequency ω of the arm. Normally, t_f decreases by increasing ω and decreasing J. Both quantities are functions of the robot arm's geometry and its physical properties. Therefore, through optimizing the arm topology, one can further decrease the traveling time obtained from the time-optimal control theory. Eventually, a minimum traveling time could be

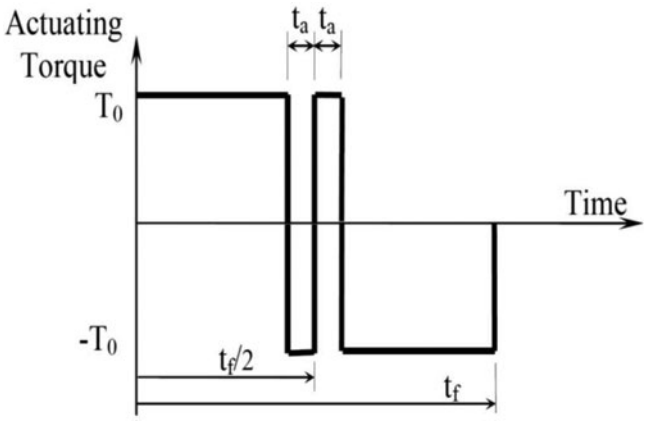

Figure 2. Bang-bang control of a flexible robot arm.

obtained based on control and structural optimization process. The treatment presented here can be readily extended to a finite number of modes, only at the expense of algebraic simplicity and mystification of the key idea. The PD controller that should follow the time-optimal control results in a stable system regardless of the number of modes. The experimental results presented in Fanni and El-Keran (2000) demonstrate the validity of using one rigid mode and one flexible mode. In addition, Hastings and Book (1987) and Wells et al. (1990) considered that "the most motion errors can be largely eliminated if only the first vibrational mode of the arm is controlled."

2.2. Mathematical model with air damping

Since the flexible robot arms should move with a very high speed, the effect of the drag force and the damping coefficient of the air have to be involved in this study. It can be modeled as an equivalent viscous damper for the rigid mode. It is clear that the air damping is negligible for the flexible mode due to its small deflection. The state equations of the air-damped flexible arm are similar to Eqs. (1) and (2), except that matrix **A** takes the following form:

$$\mathbf{A} = \begin{bmatrix} 0 & 1 & 0 & 0 \\ 0 & -\alpha & 0 & 0 \\ 0 & 0 & 0 & 1 \\ 0 & 0 & -\omega^2 & 0 \end{bmatrix} \tag{5}$$

where α is equal to the damping coefficient C divided by the mass moment of inertia of the arm J. Unlike the previous case, the solution of the Pontryagin maximum principle is a non-symmetric multi-switch bang-bang control about the middle switch, as shown in Figure 3. By applying the final state conditions, which dictate that the angular velocity must equal to zero and the angular displacement must equal to θ_o, the following equations (in a dimensionless form) are derived as:

$$1 - 2e^{-y_4/x} + 2e^{-(y_3+y_4)/x} - 2e^{-(y-y_1)/x} + 2e^{-y/x} = 0 \tag{6}$$

$$y_1 - y_2 + y_3 - y_4 - z = 0 \tag{7}$$

$$1 - 2\cos(y_4) + 2\cos(y_3 + y_4) - 2\cos(y - y_1) + \cos(y) = 0 \tag{8}$$

$$2\sin(y_4) - 2\sin(y_3 + y_4) + 2\sin(y - y_1) - \sin(y) = 0 \tag{9}$$

where the dimensionless quantities x, y_i, and z are defined as:

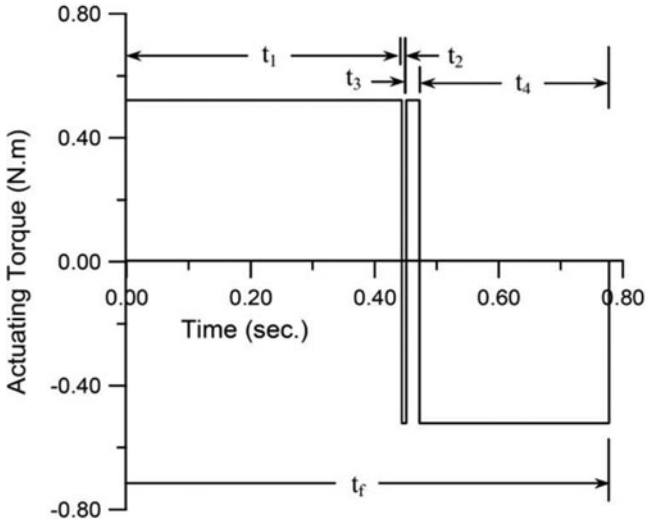

Figure 3. Torque-Time diagram for damped arm (Fanni and El-Keran 2000).

$$x = \frac{J\omega}{C}, \quad z = \frac{\omega C\theta_o}{T_o}, \quad y_i = \omega t_i, \quad \text{for}, i = 1, .., 4 \tag{10}$$

where t_i is the time interval between each two consecutive switches, then:

$$y = y_1 + y_2 + y_3 + y_4 = \omega t_f \tag{11}$$

The solution of these equations for minimum traveling time t_f is found to have the following characteristics, as noticed in Figure 3. The first and final intervals (t_1, t_4) are much larger than the inner intervals, which is quite similar to the previous case. However, the positive torque time is larger than the negative torque one (unlike the damped case, since they were equals). This is attributed to the fact that the damping torque resists the acceleration, which in turn should be compensated by more positive torque. Fanni and El-Keran (2000) presented a multi-regression technique to approximate the solution of Eqs. (6)–(9) and express the term y as a function in the quantities x and z, as follows:

$$y = \sqrt{0.4z^{2.23264} + 3.93xz} \tag{12}$$

This equation is going to be used later as the objective function for the topology optimization of the flexible arm considering the air damping effect in Section 4.2.

3. Topology optimization

Topology optimization (TO) technique strives to achieve the optimal distribution of the material within the design domain based on maximizing or minimizing certain criteria of the model under specified constraints. In general, the topology optimization algorithm selectively discretizes, removes, and relocates the elements within the design domain to achieve the optimum criteria, Rozvany (2009), Tovar et al. (2006). It provides a good layout of the structure (in such a way of minimizing the compliance or maximizing the design stiffness, …, etc.). Topology optimization has become strongly practical in many mechatronics and robotics applications, for example; optimizing the robot grippers and fingers, as presented by Zhang et al. (2019), optimizing industrial robot links, as presented by (Albert et al. 2007; Briot and Goldsztejn 2018), and many other applications stated by Wildman and Gaynor (2019). Not only in robotic fields, nowadays TO has

become a powerful aided tool in design and manufacturing systems, as demonstrated by Maranan et al. (2016).

Recently, the most popular numerical FE-based topology optimization method is Solid Isotropic Material with Penalization (SIMP), which was proposed by Bendsøe (1989). It has been initially applied for obtaining the optimal layout of trusses, as presented by Bremicker et al. (1991). The initial material properties are assumed to be constant over the entire design domain's elements. Alternatively, the continuous relative densities of the elements are used as the design variables, Bendsøe and Sigmund (2003). Each element's modulus of elasticity E_i is given as a function of the continuous relative density x_i with a power law. Hence, the material properties of the entire model are being continuously updated at each iteration in light of the following equations:

$$E_i(x_i) = E_o x_i^p \tag{13}$$

$$\rho_i(x_i) = \rho_o x_i \tag{14}$$

$$0 \le x_i \le 1, \quad i = 1, ..., n \tag{15}$$

where E_o is the initial material modulus of elasticity, ρ_i is the density for element i, ρ_o is the initial material density, n is the number of the discrete elements, and p is a penalization power to penalize the intermediate densities and force them to be solids or voids. The proper value of the penalization power can be evaluated based on Poisson's ratio ν, as derived by Bendsøe and Sigmund (1999).

The method of moving asymptotes (MMA) proposed by Svanberg (1987) has turned out to be a very efficient optimization method for both constrained and unconstrained problems in the academic and industrial fields. MMA consists of a sequence of simpler approximating sub-problems (similar to sequential linear programing SLP, and sequential quadratic programing SQP), but their approximation is based on terms of direct and reciprocal design variables. The major advantage of MMA is that these local models are convex and separable and require only one function and gradient evaluation at the iteration point. Separability here means that the necessary optimality conditions of the sub–problem do not couple the design variables. This yields to more simplicity in which, *n 1-dimensional* problems are solved instead of solving one *n-dimensional* problem. Thus, it is faster and more accurate than SLP and SQP, as investigated by Fanni et al. (2013). Convexity means that dual or primal–dual methods can be used to attack the sub-problems. More details are presented by Svanberg (2004). These valuable characteristics allow reducing the computational costs of solving the sub-problems significantly. The solution of the sub–problem is then used as the next iteration point. The general optimization problem is described in the following form:

$$\min : f_o(\mathbf{x}) \quad (\mathbf{x} \in R^n) \tag{16}$$

$$s.t. : f_i(\mathbf{x}) \le \hat{f}_i \quad \text{for} \quad i = 1, ..., m \tag{17}$$

$$\underline{x}_j \le x_j \le \bar{x}_j \quad \text{for} \quad j = 1, ..., n \tag{18}$$

where $\mathbf{x} = (x_1, ..., x_n)^T$ is a vector of the design variables, $f_o(x)$ is the objective function, $f_i(x)$ is the i^{th} constraint function, m is the number of the constraint functions, $\bar{x}_j$ and $\underline{x}_j$ are upper and lower bounds of the design variables, respectively, and n is the design variables' number.

4. Optimal integrated structural/control design

4.1. Problem formulation for topology optimization of flexible robot arm without air damping

The initial model of the robot arm is considered as a slender (aluminum 6061-T6) beam with a rectangular cross-section. The arm is attached to the motor hub in such a way that can rotate around Y-axis and move in the horizontal plane, as shown in Figure 4, so that the effect of the

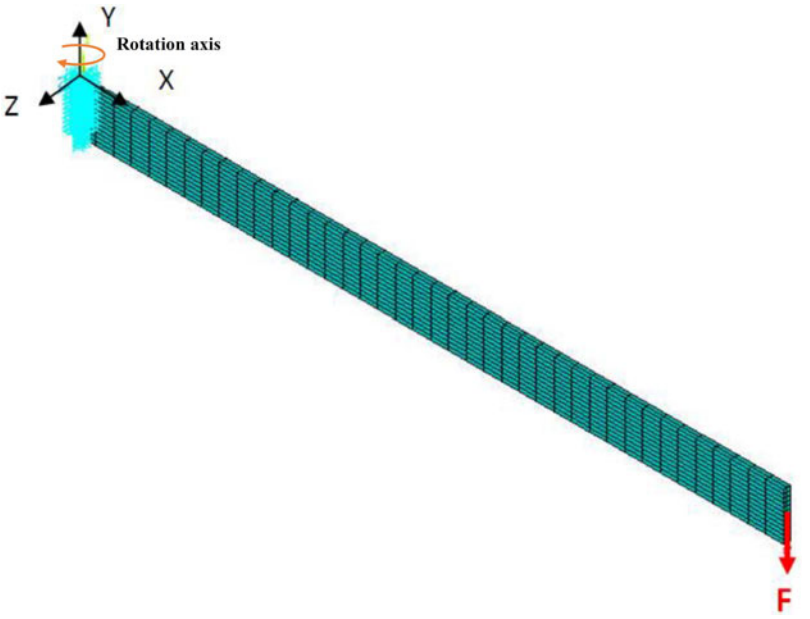

Figure 4. Initial design of high-speed flexible robot arm.

potential energy can be neglected. This arm is subjected to a payload (F) which is modeled as a concentrated mass at its tip. Different arm models based on their dimensions, material, and the effect of air damping are proposed for the optimization process, as illustrated in Table 1. The traveling time t_f resulted from the time-optimal control theory for the undamped case can be deduced from Eqs. (3) and (4) and used as the objective function in the MMA algorithm. Solving both equations yields to the following implicit form:

$$\cos\left(\frac{\omega t_f}{2}\right) - 2\cos\left(\omega\sqrt{\frac{\left(\frac{t_f}{2}\right)^2 - \frac{\theta_0 J}{T_0}}{2}}\right) + 1 = 0 \tag{19}$$

One needs to solve this equation numerically to get t_f. Since it is difficult to separate t_f at the left side, it is solved by using f_0 function in MATLAB. Then, by applying the general form of MMA method, Eqs. (16)–(18), the topology optimization problem of a flexible robot arm without air damping is formulated as follows:

$$\min: t_f(x_i) \tag{20}$$

$$s.t.: \delta(x_i) - \delta_{\max} \leq 0 \tag{21}$$

$$0 \leq x_i \leq 1 \quad \text{for} \quad i = 1, \ldots, n \tag{22}$$

where x_i is the design variable which represents the relative density of element i, and n is the number of elements. The angle θ_o and torque T_o are constant through the optimization process, as given in Table 1, while the natural frequency ω and the mass moment of inertia J are functions of the elements' relative-densities x_i. Consequently, $J(x_i)$ and $\omega(x_i)$ are calculated using the finite element method (FEM) at each iteration. The vertical deflection at the arm tip δ is constrained to be within a predefined value $\delta_{\max}$ which can be determined along with the required application's accuracy. This constraint is allocated for ensuring the rigidity of the arm. Both the topology optimization Eqs. (13)–(15) and the above main optimization algorithm (20)–(22) are integrated into the main program in order to attain an optimum robot arm layout with various holes' sizes and shapes.

Table 1. Initial parameters for different arm models.

Properties	Model I	Model II	Model III	Model IV	Model V
Material	Aluminum	Steel	Aluminum	Aluminum	Aluminum
Air damping	No	No	No	Yes	Yes
Dimensions in x, y, z (mm)	300, 20, 3	300, 20, 3	710, 38, 20	300, 20, 3	760, 20, 3
Young modulus, E (GPa)	70	207	70	70	70
Density, ρ (kg·m^3)	2700	7800	2700	2700	2700
Poisson's ratio, ν	0.33	0.3	0.33	0.33	0.33
Payload, F (g)	102	102	125	102	254.8
Applied Torque, T_o (N m)	0.2	0.2	20	0.2	0.52125
Angular displacement θ_o	180^o	180^o	20^o	180^o	180^o
Arm inertia, J_{arm} (kg·m^2)	0.00144	0.00419	0.2449	0.00144	0.0237
Hub inertia, J_{hub} (kg·m^2)	0.00047	0.00047	0.0213	0.00047	0.00071
SIMP factor (p)	3	3	3	3	3
No. of elements in (x, y, z)	40, 12, 2	40, 12, 2	50, 10, 2	40, 12, 2	50, 12, 2
Initial design value x_o	1	1	1	1	1

All the models described in the table are discretized into a certain number of 3D elements in x, y, and z directions to get adequate and satisfactory results of the material distribution, and simultaneously, not to take much computational time. MMA code written in MATLAB commands by Svanberg (2007) is utilized here. The adjustable lower and upper asymptotes' parameters of this method are beneficial and convenient with any optimization problem. The finite element analysis using ANSYS is applied and the arm is modeled by 3D solid elements called SOLID45. The inertia of the hub is modeled by a concentrated mass element called MASS21, located at a certain distance from the rotation axis of the arm. The static analysis is performed for determining the maximum deflection of the arm, while, the modal analysis is carried out for determining its eigen-frequencies. The deflection limit $\delta_{\max}$ is chosen to be 1 mm (for all models except model III and V which have 0.2 and 3.2 mm, respectively).

4.2. Problem formulation for topology optimization of flexible robot arm with air damping

The problem formulation considering the air damping has the same form as the previous case in Eqs. (20)–(22), but instead of using Eq. (19) as the traveling time, the following Eq. (23) will be used. By substituting Eqs. (10) and (11) into Eq. (12) the following t_f equation for the air damping case is obtained:

$$t_f = \frac{\sqrt{0.4\left(\frac{\theta_0 \omega C}{T_0}\right)^{2.23264} + 3.93\left(\frac{I\theta_0\omega^2}{T_0}\right)}}{\omega} \tag{23}$$

where C is the damping coefficient and it is a function of the arm dimensions as given by the following equation:

$$C = D\int_0^l r^3 W(r)\ dr \tag{24}$$

This equation is equivalent to the integration of the exposed area of each element to the air taking into consideration its location from the rotation axis. In particular, the net width $W(r)$ represents the initial width of the arm minus the widths of the voids at a certain distance r from the rotation axis. Hence, the integration is done over the entire arm length l. As the topology of the arm continuously changes, the voids' widths also change and consequently the damping coefficient does as well. D is a constant depending on the air density and the drag coefficient which has been experimentally determined to be 15.16645677 by Fanni and El-Keran (2000). Therefore, the damping coefficient $C(x_i)$ can be reinterpreted into the following form to be compatible with the discretized elements:

$$C(x_i) = D\sum_{i=1}^{n} x_i b\left[\frac{(k_i + a)^4}{4} - \frac{k_i^4}{4}\right] \tag{25}$$

where a and b are the element sizes in length and width directions, respectively, and k_i is the distance along the arm length from the rotational axis to the element i.

4.3. Sensitivity analysis

The gradient of objective and constraint functions are necessary for successfully updating the design variables required for the next iterations in order to evaluate the convergence tendency and reach the optimization goal steadily and quickly. Since, the optimization problem deals with discrete geometries, and no explicit analytical expressions for the objective and constraint functions in terms of the design variables exist, then the numerical analysis (Finite Element Method) is used to calculate the parameters needed for the objective and constraint functions (i.e., ω, J, and δ). Consequently, the differentiation of these variables with respect to x_i (i.e., $\partial\omega/\partial x_i, \partial J/\partial x_i,$ and $\partial\delta/\partial x_i$) are obtained by finite difference method in the same manner. These quantities are necessary for calculating the gradient of traveling time $\partial t_f/\partial x_i$ for the undamped and damped cases, as derived in Eqs. (26) and (27), respectively. This is accomplished by generating an internal loop within the main code to measure the effect of changing each element's relative-density on the natural frequency, inertia, and deflection. However, it consumes time since it should be repeated at each iteration, it is considered a very efficient way to get the right values of the gradients. The entire optimization process flowchart including the integration between the time-optimal control, MMA algorithm, and TO approach are shown in Figure 5.

$$\begin{aligned} &-\frac{1}{2}\sin\left(\frac{\omega t_f}{2}\right)\left(t_f\frac{\partial\omega}{\partial x_i} + \omega\frac{\partial t_f}{\partial x_i}\right) + 2\sin\left(\omega\sqrt{\frac{\left(\frac{t_f}{2}\right)^2 - \frac{\theta_o J}{T_o}}{2}}\right)\cdot \\ &\left(\frac{\partial\omega}{\partial x_i}\sqrt{\frac{\left(\frac{t_f}{2}\right)^2 - \frac{\theta_o J}{T_o}}{2}} + \frac{\frac{1}{4}\omega\left(\frac{t_f}{2}\frac{\partial t_f}{\partial x_i} - \frac{\theta_o}{T_o}\frac{\partial J}{\partial x_i}\right)}{\sqrt{\frac{\left(\frac{t_f}{2}\right)^2 - \frac{\theta_o J}{T_o}}{2}}}\right) = 0 \end{aligned} \tag{26}$$

$$\begin{aligned} \frac{\partial t_f}{\partial x_i} = \Bigg[&-\frac{\partial\omega}{\partial x_i}\sqrt{0.4\left(\frac{\theta_o\omega C}{T_o}\right)^{2.23264} + 3.93\left(\frac{J\theta_o\omega^2}{T_o}\right)} \\ &+ \left(\frac{0.5\omega}{\sqrt{0.4\left(\frac{\theta_o\omega C}{T_o}\right)^{2.23264} + 3.93\left(\frac{J\theta_o\omega^2}{T_o}\right)}}\right)\left(0.4(2.23264)\left(\frac{\theta_o\omega C}{T_o}\right)^{2.23264}\left(\frac{\theta_o}{T_o}\right)\right. \\ &\left.\cdot\left(C\frac{\partial\omega}{\partial x_i} + \omega\frac{\partial C}{\partial x_i}\right) + 3.93\left(\frac{\theta_o}{T_o}\right)\left(2J\omega\frac{\partial\omega}{\partial x_i} + \omega^2\frac{\partial J}{\partial x_i}\right)\right)\Bigg] / \omega^2 \end{aligned} \tag{27}$$

The neighborhood effect for each element is taken into consideration to eliminate the checkerboard phenomenon and filter the optimum design from the gray or black elements within the blank spaces in the design domain. This is performed by calculating the average traveling time gradient $\partial\hat{t}_f/\partial x_i$ considering the six neighbors of the element in the three principal directions, as shown in Figure 6, since the relative density of each element is affected significantly by its neighbors' values. This approach also ensure the continuity of the material distribution for the optimum design. If one or

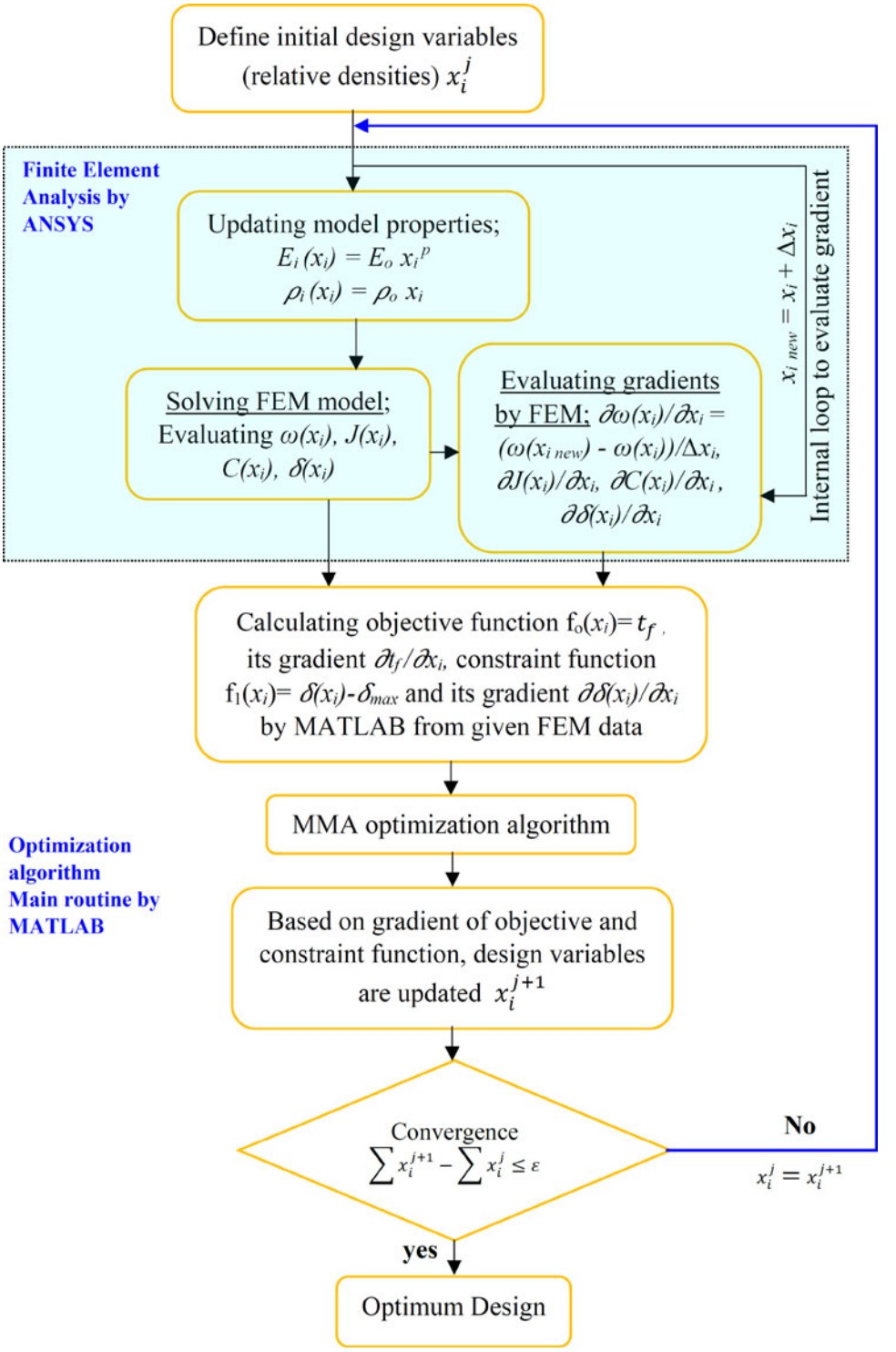

Figure 5. The proposed topology optimization flow chart of flexible robot arm.

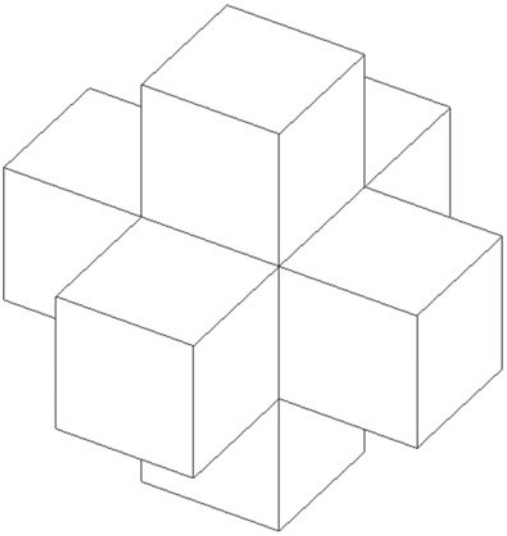

Figure 6. Element neighbors for average gradient calculation.

more neighbors do not exist at any location, they are considered null and the neighbors' number $\hat{N}$ is reduced by the same order.

$$\frac{\partial \hat{t}_f}{\partial x_i} = \left(\frac{\partial t_f}{\partial x_i} + \sum_{j=1}^{\hat{N}=6} \frac{\partial t_f}{\partial x_j} \right) / (\hat{N} + 1) \tag{28}$$

5. Results and discussions

5.1. Results of flexible robot arm without air damping effect

By applying the MMA algorithm and establishing an interface between MATLAB and ANSYS programs, the traveling time minimization can be carried out for models I, II, and III whose initial parameters are given in Table 1. Starting with model-I where the actuation torque T_o is equal to 0.20 $N \cdot m$ and the angular displacement θ_o is 180°. The initial design of the arm is a solid slender beam with very small thickness compared to its length and width, as shown previously in Figure 4. Its dimensions are $300 \times 20 \times 3$mm and its natural frequency is 49.4 Hz, the mass moment of inertia around rotation axis for the arm and hub are 0.00144 kg·m^2 and 0.00047 kg·m^2, respectively. In addition, the inertia of the payload is taken into consideration for all models. After applying the proposed algorithm and getting through 49 iterations (Supplemental video, Movie_Robot_arm_new.wmv, shows the topology progress through the optimization process), the traveling time has reduced from 0.540 sec to 0.201 sec, as shown in Figure 7. Therefore, the reduction ratio of the traveling time is about 62.7% (calculated as; *(Initial value – final value) × 100/Initial value*) which is considered as a significant reduction compared to the initial design). Another substantial improvement represented here is the reduction of arm's mass and inertia, where reducing these quantities enhance the arm performance (e.g., allowing high operation speed and reducing the sudden dynamic effect against the surroundings). The mass and inertia reduction ratio with respect to their initial values are 69.7% and 66.6%, respectively. All results of model I are presented in Table 2.

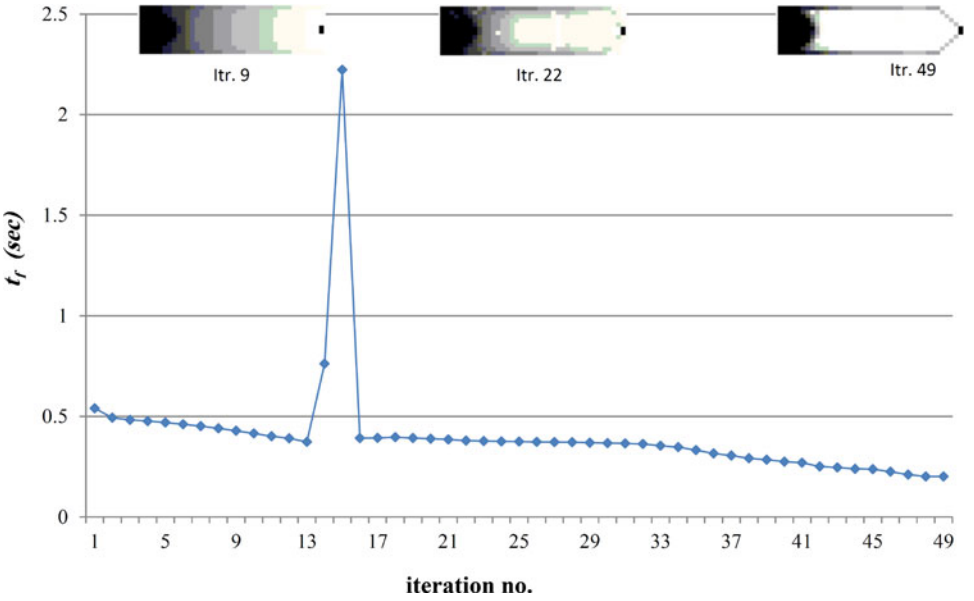

Figure 7. Traveling time of robot arm model–I vs. iteration number.

Table 2. Topology optimization results of robot arm models stated in Table 1.

	Parameters	t_f (sec)	Mass (g)	δ (mm)	$J_{Arm+hub}$ (kg·m^2)	Freq (Hz)
Model–I	Initial arm design	0.54	48.6	0.064	1.91×10^{-3}	49.4
	Final arm design	0.201	14.7	0.471	6.37×10^{-4}	34.86
	Reduction ratio %	62.7	69.7	–	85.6	–
Model–II	Initial arm design	0.628	140.4	0.022	4.66×10^{-3}	72.31
	Final arm design	0.389	26.81	0.995	6.69×10^{-4}	13.50
	Reduction ratio %	38.1	80.9	–	66.6	–
Model–III	Initial arm design	0.146	1456	0.122	0.2662	51.51
	Final arm design	0.083	439	0.198	0.0329	31.57
	Reduction ratio %	43.1	69.8	–	87.6	–
Model–IV	Initial arm design	0.343	48.6	0.064	1.910×10^{-3}	49.867
	Final arm design	0.192	11.86	0.846	5.98×10^{-4}	24.588
	Reduction ratio %	44	75.6	–	68.7	–

The optimum topological design is modeled by the CAD system, as shown in Figure 8, where the elements' relative densities are interpreted into relative thicknesses, as proposed by Sigmund and Petersson (1998). The thickness over all the design domain is variable as represented by different color contours in Figure 7. This variable thickness is taken into account while creating the CAD model in Figure 8, where it is gradually decreased from the hub toward the tip. Correspondingly, the black element means that it is totally solid (full thickness), while the gray element is an intermediate solid (part of thickness), and the white element is a void or empty material. The second model is made of steel instead of aluminum and has the same size as model–I with properties listed in Table 1. The traveling time for this arm at first iteration was 0.62 sec, and by applying the topology optimization it became 0.38 sec, with a reduction ratio of 38.1% with respect to the initial design. The final topological design is shown in Figure 9, which is quite different than the final shape of the aluminum arm. The results of the initial and final designs are given in Table 2. This example shows that the lower material density is, the lesser traveling time will be since the weight and inertia represent significant issues on such flexible robot arms. The third model is a long aluminum arm with a rectangular block hub with dimensions of $25 \times 25 \times 100$mm. The tip deflection is constrained to be within 0.2 mm. By applying

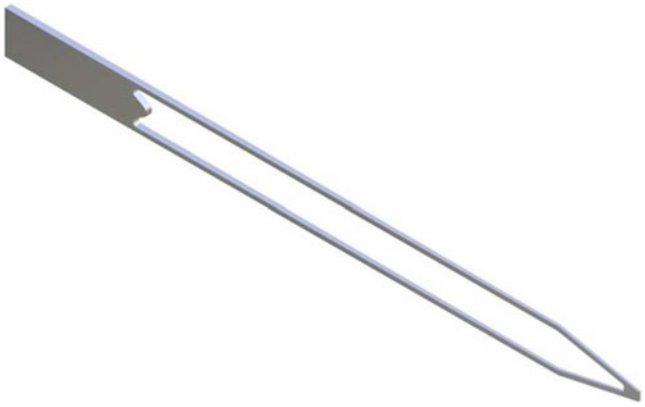

Figure 8. Final topological design of model-I (3D-modeled by solid edge).

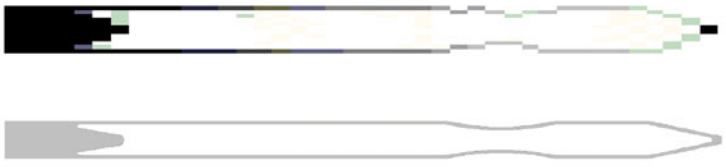

(a) The topology of the optimized arm (Up), Modeled/interpreted by Solid Edge (Down)

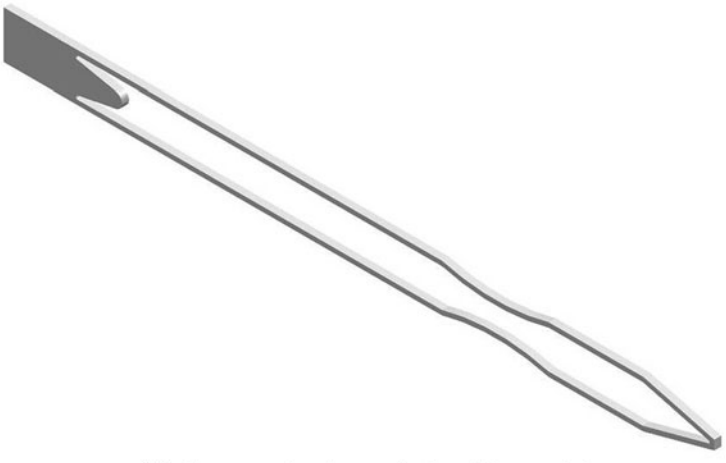

(b) Isometric view of the 3D model

Figure 9. Topology optimization of steel arm (model-II).

the topology optimization technique, it is found that t_f reduced from 0.146 to 0.083 sec. In this example, the traveling time and mass reduction ratios are 43.1% and 69.8%, respectively. All results are given in Table 2, and this Supplemental video (Arm_th20mm.wmv) shows the change of arm topology through the optimization process. The final topological design is plotted in gray-scale by Matlab and translated to 3D CAD model by Solid Edge, as shown in Figure 10.

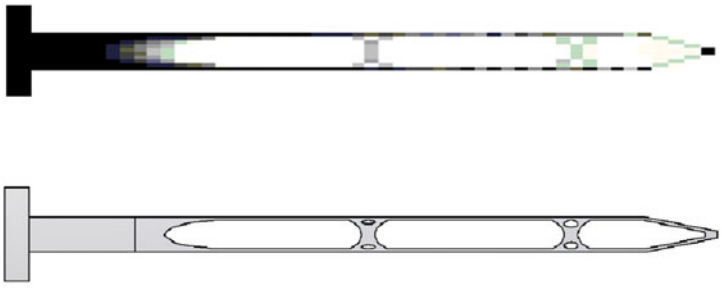

(a) Layout of the optimized arm by Matlab (Up), Modeled/interpreted by Solid Edge (Down)

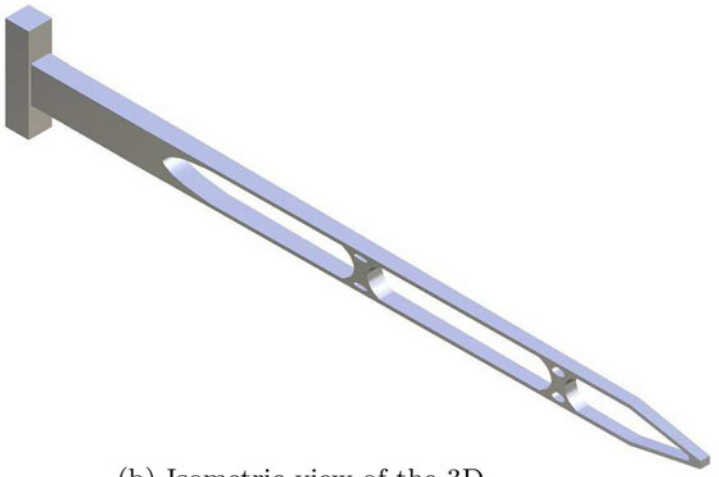

(b) Isometric view of the 3D

Figure 10. Topology optimization of long aluminum arm (model-III).

5.2. Results of flexible robot arm with air damping effect

This subsection presents the result of the robot arms subjected to air damping effect. As mentioned in Section 4.2, the traveling time is minimized using Eq. (23) instead of Eq. (19) and the deflection is constrained to be less than or equal to 1 mm. Model-IV has the same initial parameters as Model-I except taking the effect of air damping. The initial design of this model at first iteration gives a traveling time equal to 0.3435 sec, and by the completion of the optimization process, the traveling time becomes 0.1923 sec with a reduction ratio equal to 44.01%. This optimum topological model is shown in Figure 11. The mass reduction ratio of this model is equal to 75.6% which is considered a substantial improvement for an air-damped robot arm. The results of the topology optimization process are illustrated in Table 2. Although the minimum traveling time can be achieved by simultaneously decreasing the inertia and increasing the natural frequency, the results of the four models in this table show that decreasing J is the most dominant for getting the minimum t_f rather than increasing ω.

The last model to be studied here is a long aluminum arm with initial parameters stated for Model-V in Table 1. The reason behind choosing these parameters is that this model has been studied and optimized previously using size optimization technique by Fanni and El-Keran (2000). This technique has used multi-circular holes with different sizes and tried to find the best hole sizes that meet the objective function (i.e., minimizing t_f). Thus, it is beneficial to carry out the topology optimization for the same model and compare the result with both the initial design

(a) Layout of optimized arm by Matlab (Up), Modeled/interpreted by Solid Edge (Down)

(b) Isometric view of 3D model

Figure 11. Topology optimization of model-IV arm with air damping.

and the size optimization design. This will verify the feasibility and robustness of the proposed technique presented in this article. The model is divided into 50, 12 and 2 elements along x, y and z directions, respectively. Choosing the appropriate elements' number requires a compromise between the best resolution and accuracy which can be obtained and the computational time that will be consumed. The tip deflection is constrained to be less than 3.2 mm since the initial design deflection is about 3.07 mm. The payload for this model is 254.8 g and it is quite enough for carrying small objects, like a wireless camera or some objects in low-gravity space fields. A value of 0.03 is taken as a ratio between the hub and arm inertias, as specified by Fanni and El-Keran (2000). By computing the initial values for this model, it is found that the traveling time is 0.772 sec. Through the size optimization performed previously, the traveling time was minimized and has become 0.593 sec with a reduction ratio equal to 23.5%, while its mass has decreased by 33.1%. This final hollow–structure size optimization design is shown in Figure 12. On the other hand, upon applying the proposed topology optimization algorithm, t_f has become 0.426 sec with a reduction ratio of 44.8%. The dynamic simulation by ADAMS in this Supplemental video (Torque_Bang_Bang.avi) shows the bang-bang control and the relation between the applied torque (Nmm) and the time (sec). Figure 13 shows the readings of the traveling time versus the iteration number through the optimization process. Additionally, the mass of the optimized design has been reduced by 44.9%. Therefore, the topology optimization shows obviously that the traveling time and mass are reduced approximately to half of their initial values. All these results are presented in Table 3. It is preferable to include these results in a separate table apart from Table

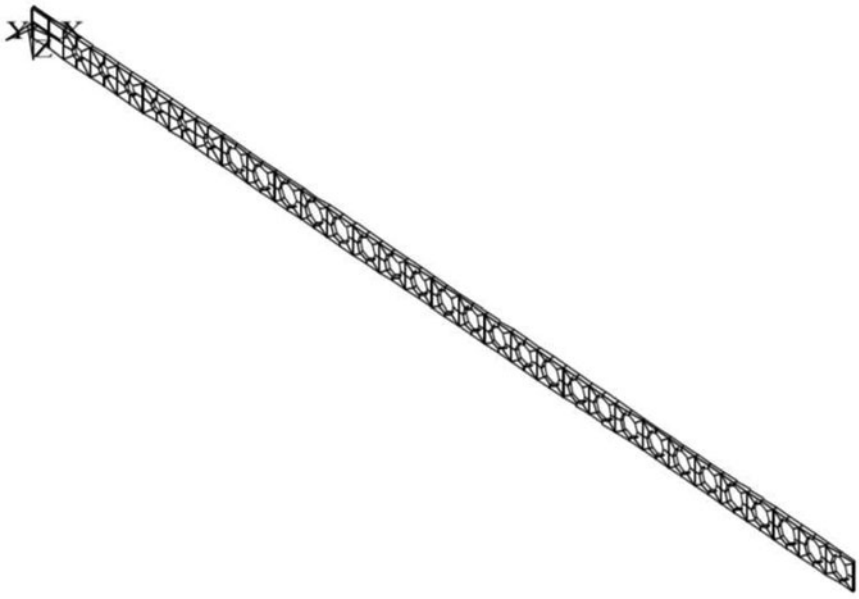

Figure 12. Optimal multi-hole structure of robot arm, model-V (760 × 20 × 3mm), considering air damping.

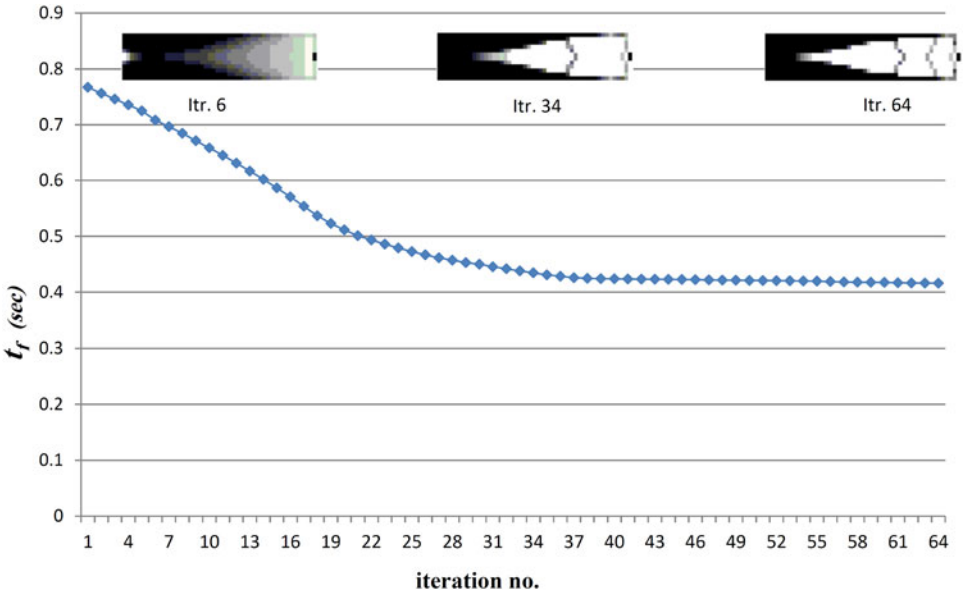

Figure 13. Traveling time of robot arm model-V vs. iteration number.

2 for clearly distinguishing between them and showing the significance of this study compared with the size optimization technique. The optimum topological design contour is plotted by Matlab and its 2D and 3D CAD models are generated by Solid Edge, as shown in Figure 14.

The bang-bang control is not very robust or accurate, therefore, a PD control is made to follow it. In order to keep the settling time of the flexible robot arm small, the first open-loop zero, first open-loop pole, open-loop gain must be kept high, as investigated experimentally by Fanni

Table 3. The results of model-V achieved by size and topology optimization w.r.t the initial design at $x_o = 1$.

	t_f (sec)	Mass (g)	δ (mm)	J_{a+h} (kg·m^2)	Freq (Hz)	C $\left(\frac{\text{N·m·s}}{\text{rad}}\right)$	K $\left(\frac{1}{\text{kg·m}^2}\right)$	P (Hz)	Z (Hz)
Initial design									
x_o=1	0.77	123.1	3.07	0.024	16.05	0.025	448.9	16.04	4.84
Size Opt.	0.59	82.36	3.20	0.014	16.3	0.015	565	16.3	5.7
− Reduc. %	23.5	33.1	–	42.6	–	40.6	–	–	–
+ Incrs. %	–	–	–	–	1.5	–	25.8	1.5	17.6
Topology	0.42	67.83	3.19	0.0075	17.27	0.009	505.3	17.27	8.82
− Reduc. %	44.8	44.9	–	69.2	–	46.2			
+ Incrs. %	–	–	–	–	7.6	–	12.5	7.6	82

(a) Layout of optimized arm by Matlab (Up), interpreted by Solid Edge (Down)

(b) 3D Isometric view of the model

Figure 14. Topology optimization of model-V with air damping.

and El-Keran (2000). Since these flexible arms are very fast, it is beneficial to integrate such control with the bang-bang control. Hence, the settling time could be greatly reduced and the desired response could be achieved steadily. The transfer function from the actuating torque to the robot arm angle is given by:

$$\frac{\theta(s)}{T(s)} = \frac{K(s^2 + Z^2)}{s^2(s^2 + P^2)} \tag{29}$$

where K is the open-loop gain, Z is the first zero, and P is the first pool, and they are given as follows:

Table 4. The results of model-V topology optimization w.r.t the initial design ($x_o = 0.551$) at the same mass.

	t_f (sec)	Mass (g)	δ (mm)	J_{a+h} (kg·m^2)	Freq (Hz)	C $\left(\frac{\text{N·m·s}}{\text{rad}}\right)$	K $\left(\frac{1}{\text{kg·m}^2}\right)$	P (Hz)	Z (Hz)
Initial design									
$x_0 = 0.551$	0.572	67.83	5.2	0.0138	14.26	0.0049	695.152	14.26	4.61
Topology	0.42	67.83	3.19	0.0075	17.27	0.009	505.3	17.27	8.82
− Reduc. %	26.5	fixed	38.6	45.6	–	–	–	–	–
+ Incrs. %	–	–	–	–	21.1	–	–	21.1	91.3

$$K = \frac{1 + qJ}{J}, \quad Z = \omega\sqrt{\frac{1}{1 + qJ}}, \quad P = \omega \tag{30}$$

As indicated in Eqs. (3) and (4), the optimal traveling time t_f decreases with the increase of ω and the decrease of J. Therefore, the optimal topological design is expected to have higher ω and lower J or at least, keep one of them within a small range around its initial value while changing the other drastically in the correct direction. Equation (30) shows that increasing ω and decreasing J (q is much smaller than 1) will increase the open-loop gain, first zero, and first pool, and hence decrease the settling time of PD control. The values of K, Z, P, and damping coefficient C at the initial, optimal size, and optimal topological designs are calculated and presented in Table 3. The increase ratios of these quantities with respect to their initial values are given in the same table showing their improvement due to the optimum topological design. Obviously, It is noticed from Table 3 that the topological design's traveling time, inertia, mass, and damping coefficient are substantially decreased too much apart from the initial and size optimization designs, in such a way that verifies the great improvement resulted from the proposed technique. For example, the reduction ratio of t_f is the double of the one obtained by size optimization. On the other hand, the first zero and pool are increased which make the PD controller settling time for the optimum design reduced greatly and ensured the stability of the system.

One can wonder what if the mass is fixed for the initial and final design, what would be the reduction ratio of the traveling time and what would be the stiffness of the arm? The proposed technique will get more credibility by comparing both initial and final designs at a fixed volume/mass fraction. This can be done by proposing that we have a model with uniformly distributed elements over the design domain with a relative density of $x_o = 0.551$ instead of $x_o = 1$. This makes the nominal design has a mass of 67.83 g which is equivalent to the final design mass. As the masses of this nominal and the final designs became equals, in this case, the proposed design's improvement can be checked according to the stiffness (reciprocal of deflection), traveling time, inertia, and natural frequency. The results presented in Table 4 show that even the masses are equals, the topology optimization has a significant achievement in reducing the traveling time (26.5%), the deflection (38.6%), and the inertia (45.6%), as well as, promoting the natural frequency (21.1%). The optimal topological design has been checked from strength viewpoint, and it is found a safe based on the static stress analysis, since, the maximum Von-Mises stress for this arm is 48.3 MPa, as shown in Figure 15, while the tensile yield strength of Al. 6061-T6 is 276 MPa. Due to the high speed and flexibility of the robot arm, it is recommended to study the dynamic stresses, as well. Subsequently, the model is passed to MSC ADAMS software to examine the maximum dynamic stress induced by the high-speed motion. This is accomplished by utilizing the AutoFlex and Durability modules in ADAMS software which is integrated with NASTRAN as FEA package to identify the magnitude of maximum dynamic stress and its location in the space, as well as, in the time frame. This analysis shows that the dynamic case has increased stress (i.e., 50.11 MPa) than the static case, as shown in Figure 16. The critical locations on the arm are at; the middle where the cross-section is the smallest, and also, at the connection between the arm and hub. These static and dynamic analyses ensure the strength of the optimized design.

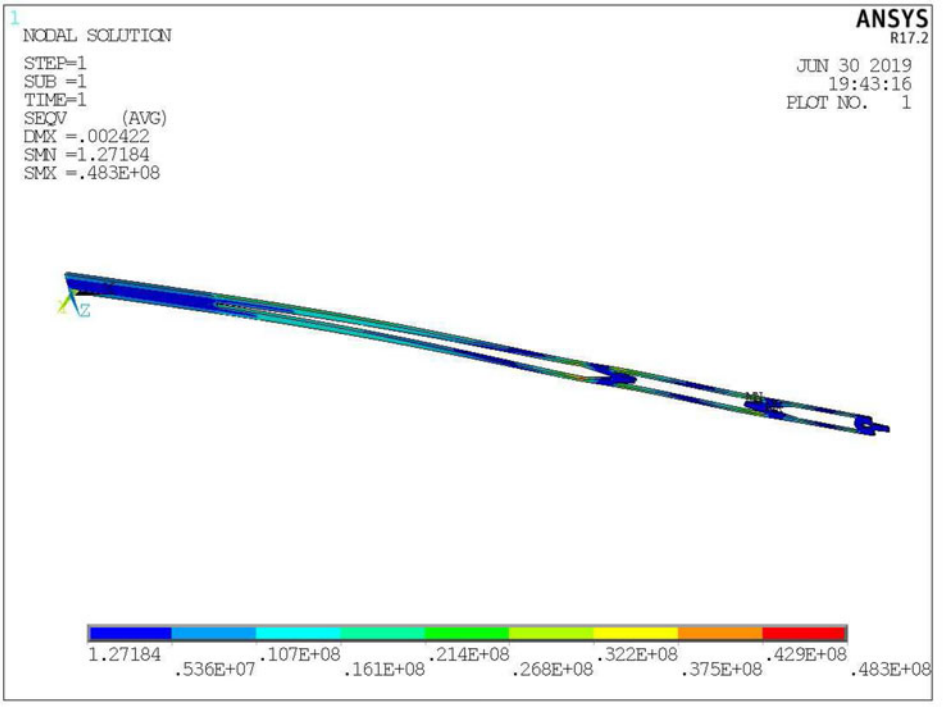

(a) Stress Analysis of Model–V

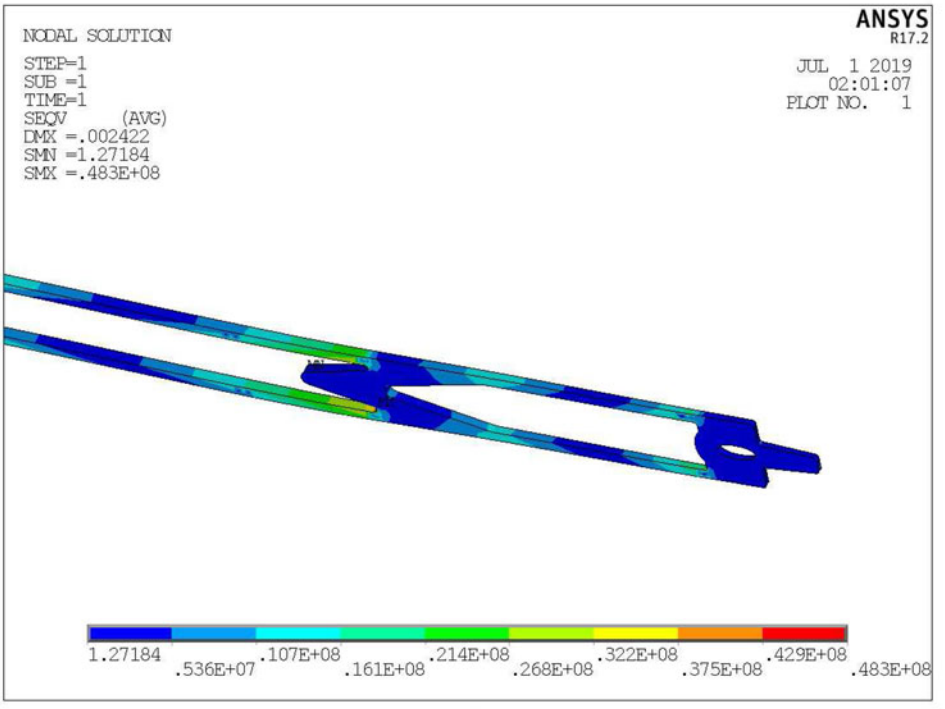

(b) Zoom view of the maximum stress region

Figure 15. Static finite element analysis of model–V using ANSYS.

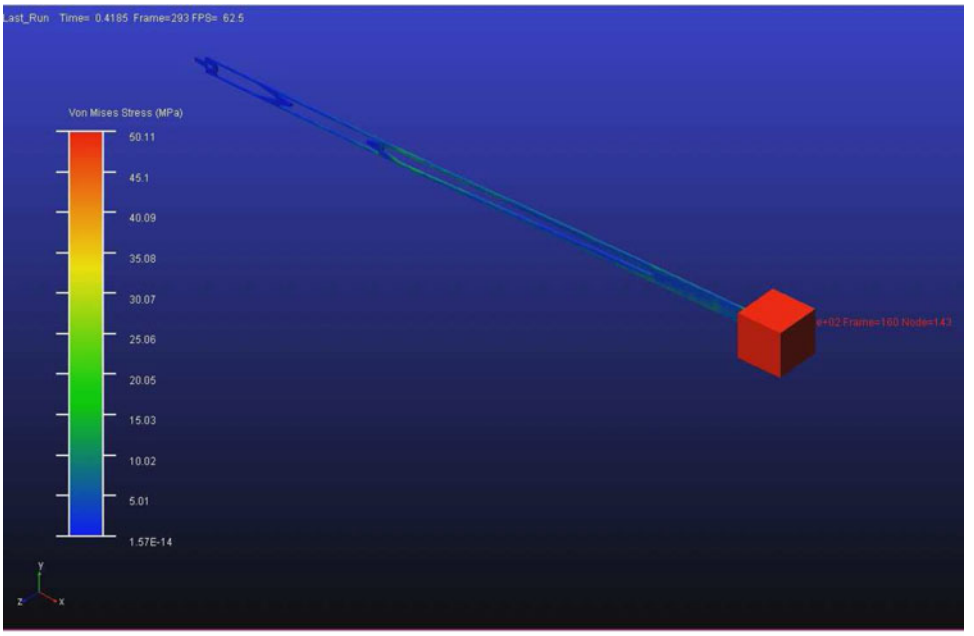

(a)

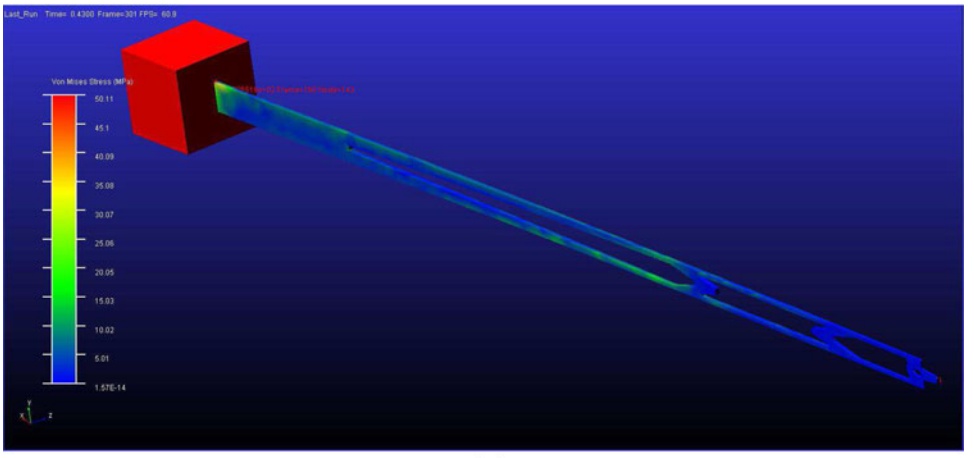

(b)

Figure 16. Dynamic stress analysis of model–V using ADMAS/NASTRAN (Supplemental animation video, stress_analysis.avi).

6. Conclusions

The flexible robot arms have significant importance not only in the industrial fields which require high operation arms like parallel robots, but also, in the space robotic fields where very light-weight arms for the low-gravity environments are needed. In this article, a methodology for the optimum topology design of high-speed flexible robotic arm is proposed. The purpose of this study is to utilize the merits of modern structural optimization and control techniques simultaneously for obtaining a minimum traveling time for the robot arm. All the studied models show that the traveling time has reduced substantially to about half of its initial value, (e.g., 44.8% for air damped example and 62.7% for undamped one). It is noticed that all the optimized models have a gradual reduced thickness toward the tip. The proposed optimal topology of the robot

arm outperforms the previously performed size optimization of the same robot arm with consideration of air damping. The reduction ratio of the topology optimization design is nearly twice that of the corresponding multi-holes size optimization. The proposed technique can be extended for studying any number of flexible modes and considering multi-flexible links of the robot arm.

Acknowledgements

The authors gratefully thank Professor Krister Svanberg, Royal Institute of Technology, Stockholm, for providing us with his MMA optimization subroutine. Also, we are so grateful to the anonymous reviewers of this article whose valuable comments have enriched it.

ORCID

Mohamed G. Alkalla http://orcid.org/0000-0001-5264-3292

References

Albert, A., O. Jens, M. Johannes, and H. Pascal. 2007. Topology optimization in mechatronic systems. Guidelines for a Decision Support Method Adapted to NPD Processes.

Asada, H., Z.-D. Ma, and H. Tokumaru. 1990. Inverse dynamics of flexible robot arms: Modeling and computation for trajectory control. *Journal of Dynamic Systems, Measurement, and Control* 112 (2):177–85. doi:10.1115/1.2896124.

Asada, H., J. Park, and S. Rai. 1991. A control-configured flexible arm: Integrated structure control design. Proceedings of 1991 IEEE International Conference on Robotics and Automation, Vol. 3, 2356–62.

Bendsøe, M. P. 1989. Optimal shape design as a material distribution problem. *Structural Optimization* 1 (4): 193–202. doi:10.1007/BF01650949.

Bendsøe, M. P., and O. Sigmund. 1999. Material interpolation schemes in topology optimization. *Archive of Applied Mechanics* 69 (9–10):635–54. doi:10.1007/s004190050248.

Bendsøe, M. P., and O. Sigmund. 2003. *Topology optimization: Theory, methods and applications, handbook*, 1–13. Berlin, Heidelberg: Springer-Verlag.

Bhattacharya, S., G. K. Ananthasuresh, and A. Ghosal. 2018. Design of a one-dimensional flexible structure for desired load-bearing capability and axial displacement. *Mechanics Based Design of Structures and Machines* 46 (3):376–99. doi:10.1080/15397734.2018.1439755.

Bremicker, M., M. Chirehdast, N. Kikuchi, and P. Y. Papalambros. 1991. Integrated topology and shape optimization in structural design. *Mechanics of Structures and Machines* 19 (4):551–87. doi:10.1080/08905459108905156.

Briot, S., and A. Goldsztejn. 2018. Topology optimization of industrial robots: Application to a five-bar mechanism. *Mechanism and Machine Theory* 120:30–56. doi:10.1016/j.mechmachtheory.2017.09.011.

Carrera, E., and M. A. Serna. 1996. Inverse dynamics of flexible robots. *Mathematics and Computers in Simulation* 41 (5–6):485–508. Robotics and intelligent systems. doi:10.1016/0378-4754(95)00095-X.

De Luca, A. 2000. Feedforward/feedback laws for the control of flexible robots. Proceedings of 2000 ICRA. Millennium Conference. IEEE International Conference on Robotics and Automation. Symposia Proceedings (Cat. No. 00CH37065), Vol. 1, 233–40.

De Luca, A., and R. De Simone. 1997. Controllo di traiettoria per robot con bracci flessibili basato sull'inversione in frequenza della dinamica. 41 Conv. ANIPLA (Automation 1997), 227–36.

De Luca, A., L. Lanari, P. Lucibello, S. Panzieri, and G. Ulivi. 1990. Control experiments on a two-link robot with a flexible forearm. 29th IEEE Conference on Decision and Control, 520–7. IEEE.

Dixit, U., R. Kumar, and S. Dwivedy. 2006. Shape optimization of flexible robotic manipulators. *Journal of Mechanical Design* 128 (3):559–65. doi:10.1115/1.2181606.

Dong, J., B. He, M. Ming, C. Zhang, and G. Li. 2019. Design of open-closed-loop iterative learning control with variable stiffness for multiple flexible manipulator robot systems. *IEEE Access* 7:23163–8. doi:10.1109/ACCESS.2019.2898266.

Fanni, M. 2000. Time-optimal control of high-speed flexible-robot arm using pd algorithms. *Engineering Journal of Qatar University* 13:291–305.

Fanni, M., and A. El-Keran. 2000. Theoretical and experimental investigation of integrated structure control design of high speed flexible robot arm. Current Advances in Mechanical Design and Production, 7th Cairo University International MDP Conference, 45–56.

Fanni, M., M. Shabara, and M. Alkalla. 2013. A comparison between different topology optimization methods. *Mansoura Engineering Journal, MEJ* 38 (1).

Gao, Y., and F.-Y. Wang. 2003. *Advanced studies of flexible robotic manipulators: Modeling, design, control, and applications*. Vol. 4. Singapore: World Scientific.

Ghazavi, A., and F. Gordaninejad. 1995. A comparison of the control of a flexible robot arm constructed from graphite/epoxy versus aluminum. *Computers & Structures* 54 (4):621–32. doi:10.1016/0045-7949(94)00375-D.

Hastings, G., and W. Book. 1987. A linear dynamic model for flexible robotic manipulators. *IEEE Control Systems Magazine* 7 (1):61–4.

Hong, S.-M., and Y. Sik Park. 1999. Vibration reduction of flexible manipulators using torque wheels. *Mechanics of Structures and Machines* 27 (1):1–22.

Imam, I., and G. N. Sandor. 1975. High-speed mechanism design – A general analytical approach. *Journal of Manufacturing Science and Engineering* 97 (2):609–28.

Kayastha, S., J. Katupitiya, and G. Pearce. 2018. Control of a space robot with flexible manipulator using generalized decoupling technique. In 2018 2nd International Conference on Robotics and Automation Sciences (ICRAS), 1–6.

Lai, H.-J., and B. Dopker. 1990. The influence of lumped rotary inertia in flexible multibody dynamics. *Mechanics of Structures and Machines* 18 (2):197–210.

Maranan, V., T. W. Simpson, T. Palmer, C. J. Dickman, S. N. Reddy K. 2016. Application of topology optimization and design for additive manufacturing guidelines on an automotive component. ASME 2016 International Design Engineering Technical Conferences and Computers and Information in Engineering Conference, pp. V02AT03A030–V02AT03A030. American Society of Mechanical Engineers.

Pao, L. Y., and G. F. Franklin. 1990. Time-optimal control of flexible structures. In 29th IEEE Conference on Decision and Control, Vol. 5, 2580–1.

Park, J.-H., and H. Asada. 1994. Concurrent design optimization of mechanical structure and control for high speed robots. *Journal of Dynamic Systems, Measurement, and Control* 116 (3):344–56.

Rozvany, G. 2009. A critical review of established methods of structural topology optimization. *Structural and Multidisciplinary Optimization* 37 (3):217–37.

Sigmund, O., and J. Petersson. 1998. Numerical instabilities in topology optimization: A survey on procedures dealing with checkerboards, mesh-dependencies and local minima. *Structural Optimization* 16 (1):68–75.

Svanberg, K. 1987. The method of moving asymptotesa new method for structural optimization. *International Journal for Numerical Methods in Engineering* 24 (2):359–73.

Svanberg, K. 2004. Some modelling aspects for the Matlab implementation of MMA. requested by e-mail.

Svanberg, K. 2007. Matlab MMA–code. requested by e-mail.

Tovar, A., N. M. Patel, G. L. Niebur, M. Sen, and J. E. Renaud. 2006. Topology optimization using a hybrid cellular automaton method with local control rules. *Journal of Mechanical Design* 128 (6):1205–16.

Wells, R. L., J. K. Schueller, and J. Tlusty. 1990. Feedforward and feedback control of a flexible robotic arm. *IEEE Control Systems Magazine* 10 (1):9–15.

Wildman, R., and A. Gaynor. 2019. Topology optimization for robotics applications. In *Robotic systems and autonomous platforms*, eds. S. M. Walsh and M. Strano, 251–92. Sawston: Woodhead Publishing.

Yamaguchi, K., T. Endo, Y. Kawai, and F. Matsuno. 2018, September. Contact-force control of one-link flexible arm without using physical parameters in the controller design. 2018 12th France-Japan and 10th Europe-Asia Congress on Mechatronics, 195–200.

Zhang, H., A. S. Kumar, F. Chen, J. Y. H. Fuh, and M. Y. Wang. 2019. Topology optimized multimaterial soft fingers for applications on grippers, rehabilitation, and artificial hands. *IEEE/ASME Transactions on Mechatronics* 24 (1):120–31.

Zhang, J., Y. Ma, Z. Zhao, and X. He. 2018. Control design of a vibrating flexible timoshenko robot arm with restricted input. 2018 3rd International Conference on Advanced Robotics and Mechatronics (ICARM), 213–8.

Zhang, W. 2018. The impulse spectrum method for vibration suppression of a flexible multilink robot arm. *Journal of Vibration and Control* 24 (17):3865–81.